Comparisons of Compressible and Incompressible Solvers: Flat Plate Boundary Layer and NACA airfoils

Moritz Kompenhans[1], Esteban Ferrer[2], Gonzalo Rubio, Eusebio Valero

E.T.S.I.A. (School of Aeronautics)

Universidad Politécnica de Madrid

[1] moritz.kompenhans@upm.es

[2] esteban.ferrer@upm.es

June 27, 2013

Abstract

This paper presents comparisons of high order Discontinuous Galerkin (DG) solvers using both compressible and incompressible formulations for the solution of the Navier-Stokes equations. The main purpose of this paper is to provide qualitative and quantitative comparisons to assess the limits of accuracy of compressible solvers when computing low Reynolds and low Mach number flows. Comparisons encompass flow simulations for two test-cases included in the *2nd International Workshop on High Order Methods* May 27 - 28, 2013 to be held in Cologne, Germany: "C1.3 Flow over the NACA0012 airfoil" and "C1.4 Flat plate Boundary Layer". Both high order codes provide h/p refinement capabilities and enable grid independent flow comparisons using either h or p refinement. Namely, drag coefficients and boundary layer profiles (e.g. displacement thickness) are compared together with theoretical estimates, when available (e.g. Blasius solution). It is shown that both compressible and incompressible formulations provide similar results even at low Reynolds numbers. However, this paper shows that the accuracy of the compressible computations is inversely proportional to both Reynolds and Mach numbers and quantifies these

differences for the test cases considered. Finally, we show that compressible solvers, when utilised under incompressible flow conditions (i.e. using low Mach numbers without corrections or preconditioning) do not provide the same lift and drag coefficients than incompressible solvers.

1 Codes description

This section presents a brief overview of the solvers used for the comparisons presented in this work. Both high order DG compressible and incompressible formulations share the suitable characteristic of minimising spatial numerical errors and hence enable comparisons of flow formulations. In addition, let us note that both codes use the non-dimensional form of the respective NS equations.

1.1 Compressible solver

A nodal explicit 2D high order DG code based on the DGSEM formulation [5] has been used to provide results for compressible flows. To increase the flexibility of the solver a mortar element method is used to couple the element faces if hanging nodes or elements with varying polynomial orders are used in the computational mesh. Temporal advancement is provided by a 3rd Order Runge Kutta scheme. One of the code's main capabilities is the possibility to perform automatic local spatial adaption (using either h or p refinement) based on τ-error estimates, Rubio et al. [6]. However, this capability is not used here. The code uses OpenMP parallelisation with shared memory.

1.2 Incompressible solver

Flow solutions of the 3D incompressible NS equations, are obtained from the unsteady high order h/p DG - Fourier solver developed by Ferrer and detailed in [2], [3] and [1]. This high order solver provides highly accurate solutions on static and moving domains composed of mixed triangular-quadrilateral meshes and can cope with curved boundary elements. A mixed implicit-explicit second order stiffly stable method is used to discretise in the NS equations in time whilst spatial discretisation is provided by the DG - Symmetric Interior Penalty Galerkin formulation with modal basis functions in

the x-y plane. Spatial discretisation in the z-direction is provided by a purely spectral method that uses Fourier series and allows computation of spanwise periodic three-dimensional flows. The code is parallelised for distributed memory clusters using a a combination of MPI and OpenMP paradigms.
The solver has been widely validated for a variety of flows, including bluff body flows, airfoil and blade aerodynamics under static and rotating conditions [3] [1].
In this paper all computations performed using the incompressible solver are limited to 2D .

2 Case Summary

We present results for two test cases: "C1.3 Flow over the NACA0012 airfoil" and "C1.4 Flat plate Boundary Layer". In addition to the flow conditions specified by the workshop organisers, we include lower Reynolds numers and various low Mach numbers to study the differences between compressible and incompressible formulations. A summary of the various cases is provided in Table 1.

Case	Reynolds	Mach	AOA
Boundary Layer Compressible solver	60, 600, 3600	0.05, 0.1, 0.3	-
Boundary Layer Incompressible solver	60, 600	-	-
NACA0012 Compressible solver	5000	0.5	1°
NACA0015 Compressible solver	100	0.2, 0.3	0°
NACA0015 Incompressible solver	100	-	0°

Table 1: Summary of test cases detailing Reynolds number, Mach number and Angle of Attack (AOA).

The calculations presented in this work have been performed on a 64 Beowulf cluster based on 8 quad-core Intel Xeon processor with nominal speed of 2.40GHz. Taubench is running in 10.265 seconds in one core. The authors follow the workshop requirement to calculate the converged solutions. Both, compressible and incompressible solution are started from a uniform free stream and are advanced in time until a steady state solution is reached.

3 Meshes

3.1 C1.4. Laminar Boundary Layer on a Flat Plate

For the Flat Plate Boundary Layer Simulation (see Figure 2) a domain of $L_X = 10$ and $L_Y = 5$ is used while the Plate has a length of $L_P = 6$ and is preceded by a symmetry region of length $L_H = 4$. The current unstructured grid for the compressible solver is shown in Figure 2 (a). The grid for the compressible solver was generated by the in house software SpecMesh2D and Gambit [4] was used to generate the meshes for the incompressible solver (see Figure 2.b).

3.2 C1.3. Flow over NACA0012 and NACA0015 Airfoils

Figure 1 shows examples of the grids used for compressible and incompressible formulations for a NACA0015. The left triangular mesh is used by the incompressible solver whilst the quadrilateral mesh, on the right, is used by the compressible code. Let us note that the calculations for the NACA0012 are performed in similar grids.

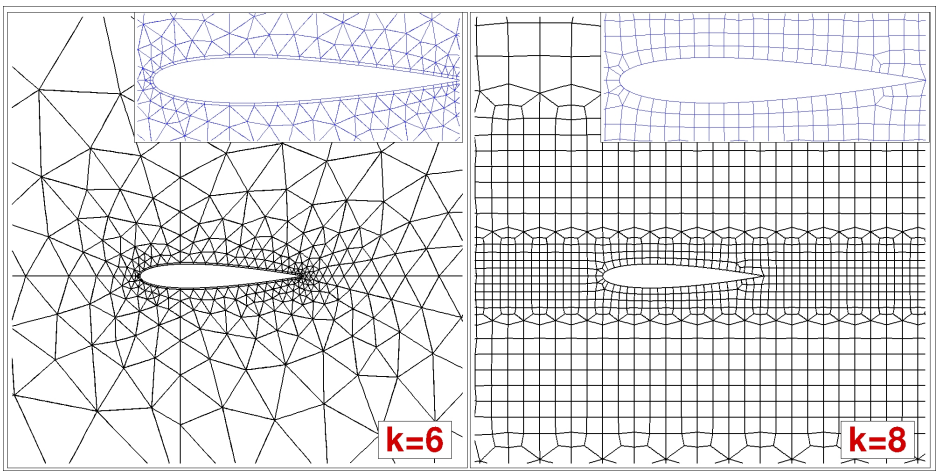

Figure 1: NACA0015 airfoil meshes using triangles for the incompressible and quadrilaterals for the compressible solver

4 Results and Comparisons

4.1 C1.4. Laminar Boundary Layer on a Flat Plate

Figure 2.a shows streamwise velocity contours obtained by the compressible solver on a quadrilateral grid and Figure 2.b shows the streamwise velocity contours obtained using the incompressible solver with a tetrahedral grid. The polynomial order for the compressible solver was set to $k = 8$ in all elements in x and y direction, whilst $k = 11$ was used for the incompressible calculations.

Non-dimensional velocity profiles for the compressible and the incompressible boundary layer formulations are compared in Figure 3. The Figure shows the velocity profiles at a distance of $L = 5.2$ downstream from the leading edge at a Reynolds number of $Re_L = 520$. The calculations of the compressible solver were accomplished for different Mach numbers and compared to the incompressible and the Blasius solution (see Schlichting [7]). Table 2 summarizes the viscous contributions for the drag coefficient c_{Dv} computed with both solvers together with Blasius analytical estimates: $c_{D_v} = \frac{1.328}{\sqrt{Re_{L_p}}}$. Furthermore, we define the error as the relative difference with respect to the incompressible solution as:

$$Error_{c_{D_v}} = \left| \frac{c_{D_v}^{Compressible} - c_{D_v}^{Incompressible}}{c_{D_v}^{Incompressible}} \right| \times 100 \ ,$$

and include this error in the table 2. In addition, the boundary layer thicknesses $\delta_1^{Re_L} = \int_0^\infty (1 - \frac{U}{U_\infty}) dy$ are compared.
When comparing the drag coefficient at the lowest Reynolds (i.e. $\mathrm{Re}_{L_p} = 60$), the table shows that incompressible and compressible solutions using the lowest Mach number provide similar results: 1.4% error. However, the time step needed to achieve converged solutions using the compressible solver, where an exlpicit time advancement scheme is used, are 100-times smaller (i.e. longer computation). At $\mathrm{Re}_{L_p} = 600$ all computations show similar errors when compared to the incompressible results. The discrepancies between computed results and boundary layer drag coefficient obtained from Blasius may be explained by the singularity at the plate leading edge, which is not taken into account by the Blasius theory, Schlichting [7].
Comparing the boundary layer thickness, it can be seen that the incompressible solver provides more accurate results than the compressible solver.

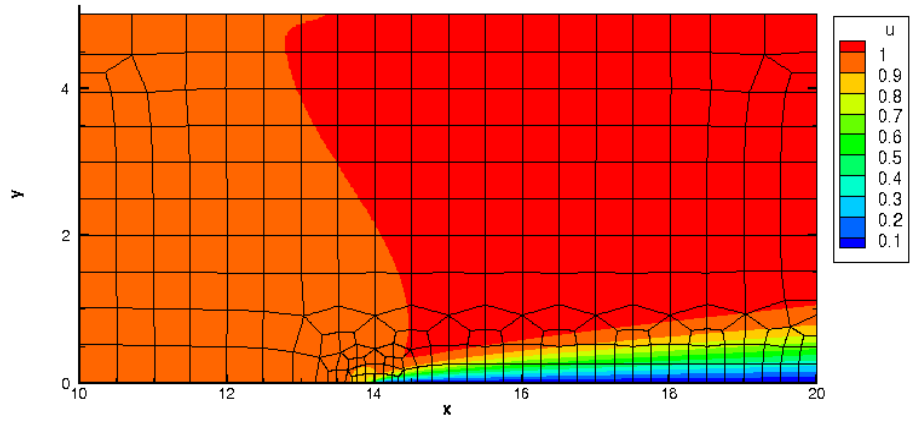

(a) Flowfield of streamwise velocity using the compressible solver; quadrilateral grid; polynomial order k=8.

u

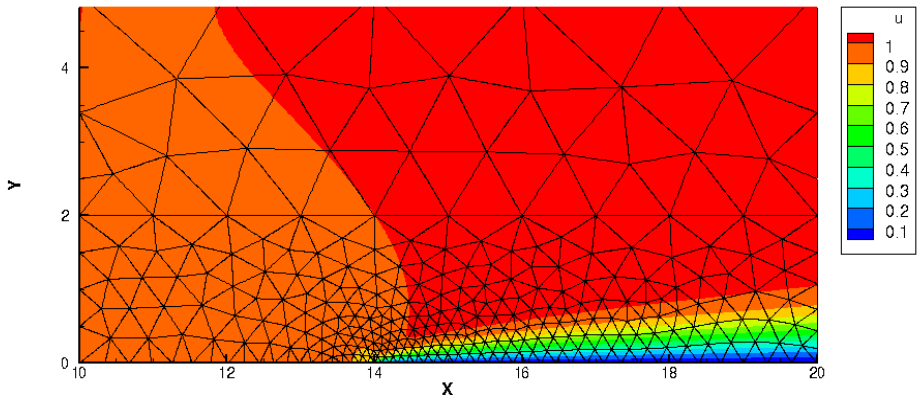

(b) Flowfield of streamwise velocity using the incompressible solver; tetrahedral grid; polynomial order k=11.

Figure 2: Comparison of compressible and incompressible solvers on a Boundary Layer; streamwise-velocity for $\mathrm{Re}_{L_p} = 600$

Furthermore, it can be recognized that the compressible solution with the lowest Mach number is the most accurate one of the compressible results. Figure 4 shows the drag error for different polynomial orders and the respec-

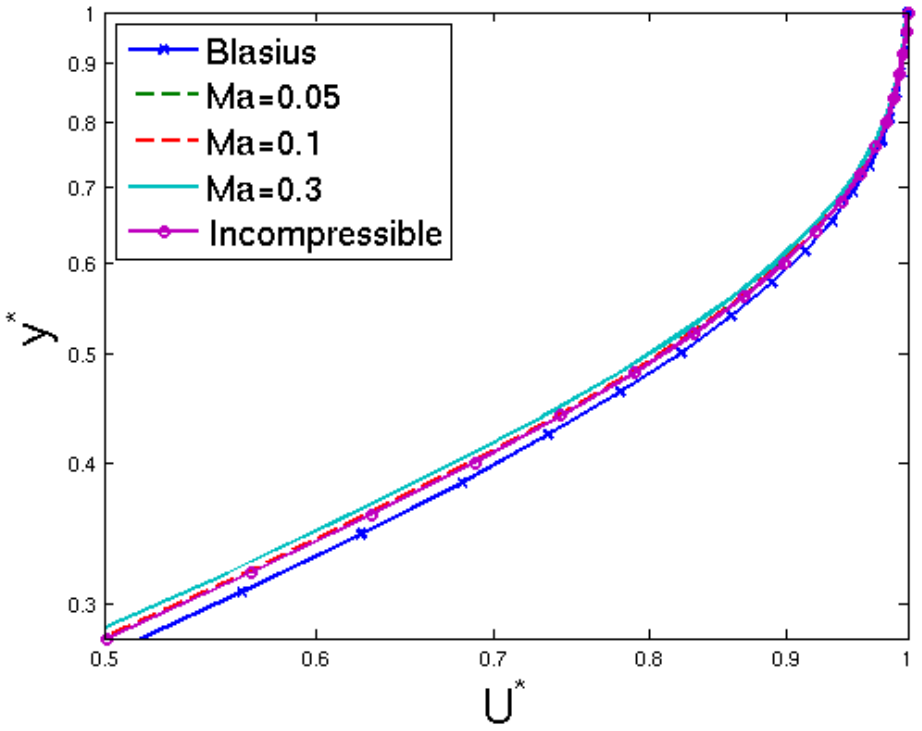

Figure 3: Velocity profiles at a distance of $L = 5.2$ downstream from the leading edge at a Reynolds number of $\mathrm{Re}_L = 520$

tive work units for two grids including their respective degrees of freedom.

4.2 C1.3. Flow over a NACA0012 and NACA0015 Airfoil

4.2.1 NACA0012

Figure 5 shows the result the NACA0012 provided by the compressible solver at $\mathrm{Re}_c = 5000$, $\mathrm{Ma} = 0.5$ and $\alpha = 1°$, as defined in the workshop. As expected p-refinement, Figure 5.a, shows an exponential scaling for higher degrees of freedom in terms of accuracy and work units. When performing h-refinement, as shown in Figure 5.b, for a polynomial order $k = 6$, it can be seen a slope

	$\mathrm{Re}_{L_p} = 60$		$\mathrm{Re}_{L_p} = 600$			
	c_{D_v}	$error_{c_{D_v}}[\%]$	c_{D_v}	$error_{c_{D_v}}[\%]$	$\delta_1^{Re_L}$	$error_{\delta_1^{Re_L}}[\%]$
Incompressible	0.22266	-	0.06039	-	0.3097	-
Ma = 0.05	0.21934	1.49	0.05967	1.20	0.3105	0.28
Ma = 0.1	0.23031	3.43	0.05956	1.38	0.3113	0.51
Ma = 0.3	0.26267	17.97	0.05978	1.01	0.3164	2.18
Blasius	0.17144	23.00	0.05421	10.23	0.3022	2.42

Table 2: Viscous drag-coefficients c_{D_v} at $\mathrm{Re}_{L_p} = 60$ and $\mathrm{Re}_{L_p} = 600$ for compressible, incompressible and Blasius solution. In addition, results fo the displacement thickness $\delta_1^{Re_L=520}$ are summarised

of 7.25 confirming that the order of accuracy h^{k+1}, where h defines the mesh size and k the polynomial order, is achieved.

4.2.2 NACA0015

Additional comparisons between the compressible and the incompressible solvers have been performed for the NACA0015 airfoil at $\mathrm{Re}_c = 100$ and zero Angle of Attack $\alpha = 0°$, for two Mach numbers ($\mathrm{Ma} = 0.2, 0.3$) . Compressible solution have been obtained using a polynomial order $k = 8$, whilst incompressible results are obtained with $k = 6$. These results are summarised in Table 3. The table shows that even when low Mach numbers are considered, there is a considerable difference between the compressible and incompressible results for both viscous and pressure components of the drag coefficient. In addition, let us note that these differences increase when incrementing the Mach number. For completeness, we include in Figure 6 a comparison of the pressure and skin friction coefficients. It can be seen that both code agree very well overall. Minor differences are seen near the leading edge for the skin friction plot, which may be due to lack of local spatial resolution but this difference is still under investigation.

Conclusions

This paper includes comparisons of compressible and incompressible high order discontinuous Galerkin solvers for two test cases included in the *2nd Inter-*

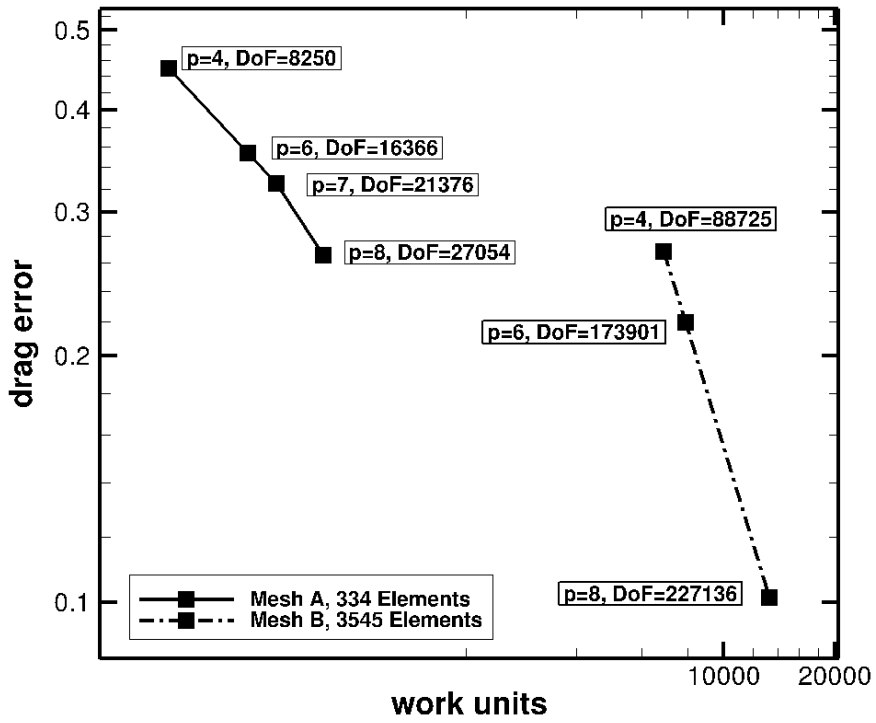

Figure 4: L^2 norm of the relative error for the drag coefficient: flat plate at $\mathrm{Re}_{L_p} = 3600$

	c_{D_p}	c_{D_v}	c_D	$errorc_{D_p}[\%]$	$errorc_{D_v}[\%]$	$errorc_D[\%]$
Incompressible	0.2044	0.3402	0.5446	-	-	-
Ma = 0.2	0.2104	0.3538	0.5642	2.90	4.00	3.59
Ma = 0.3	0.2192	0.3691	0.5883	7.22	8.51	8.02

Table 3: NACA0015 at $\mathrm{Re}_c = 100$ and $\alpha = 0°$. Drag-coefficients $c_D = c_{D_p} + c_{D_v}$, including pressure c_{D_p} and viscous c_{D_v} components, for the compressible and incompressible solvers

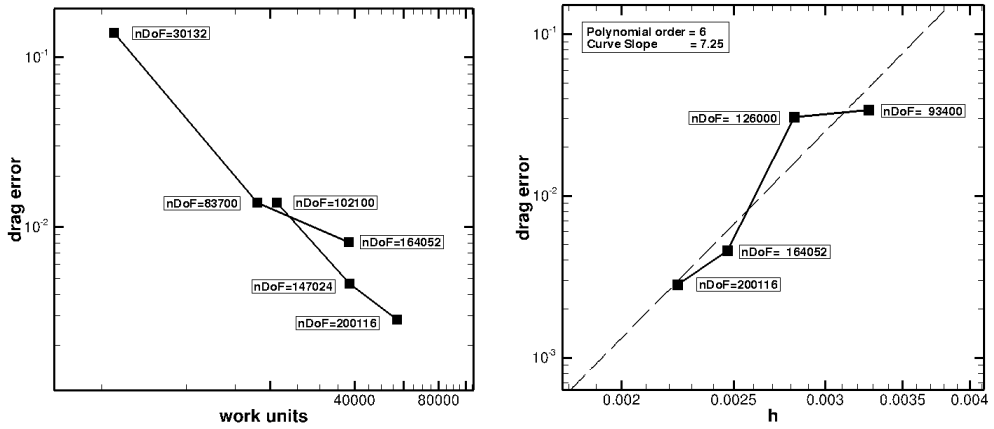

(a) p-refinement (b) h-refinement

Figure 5: L^2 norm of the relative error for the drag coefficient: h/p refinement for a NACA0012 at Re=5000

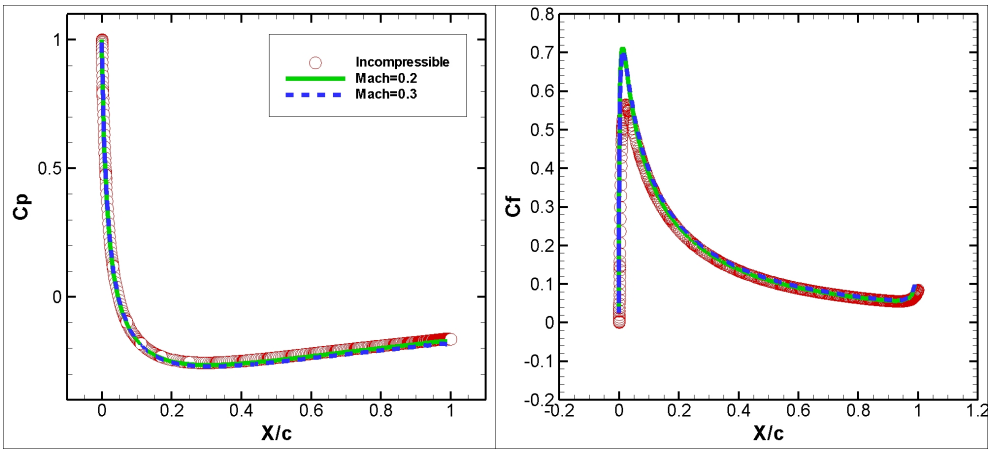

Figure 6: Pressure (Cp) and skin friction (Cf) coefficients for a NACA0015 at Re=100 using compressible and incompressible solvers

national Workshop on High Order Methods: "C1.3 Flow over the NACA0012 airfoil" and "C1.4 Flat plate Boundary Layer". It is shown that the compressible results approach the incompressible solutions as the Reynolds increases. For low Reynolds number, the Mach number is required to decrease in or-

der for both solvers to provide similar results in lift and drag coefficients. In addition, we show that compressible solvers when running under incompressible flow conditions (i.e. using low Mach numbers without corrections or preconditioning) do not provide the same aerodynamic quantities than incompressible solvers. These results provide some guidelines and error estimates that quantify these differences and may need to be considered when running compressible solvers at incompressible flow regimes.

Acknowledgements

The authors would like to thank the support of the European Commission for the financial support of the ANADE project under grant contract PITN-GA-289428.

References

[1] E. Ferrer. *A high order Discontinuous Galerkin - Fourier incompressible 3D Navier-Stokes solver with rotating sliding meshes for simulating cross-flow turbines*. PhD thesis, University of Oxford, 2012.

[2] E. Ferrer and R.H.J. Willden. A high order discontinuous Galerkin finite element solver for the incompressible Navier–Stokes equations. *Computers & Fluids*, 46(1):224–230, 2011.

[3] E. Ferrer and R.H.J. Willden. A high order discontinuous galerkin - fourier incompressible 3d navier-stokes solver with rotating sliding meshes. *Journal of Computational Physics*, 231(21):7037–7056, 2012.

[4] Fluent Ansys Inc. Gambit users guide. *Lebanon NH*, 1998.

[5] D. A. Kopriva. *Implementing Spectral Methods for Partial Differential Equations: Algorithms for Scientists and Engineers*. Springer Publishing Company, 1st edition, 2009.

[6] G. Rubio, E. Valero, F. Fraysse, and J. deVicente. The estimation of truncation error by τ-estimation for chebyshev spectral collocation method. *Journal of Scientific Computing (accepted for publication)*, 2013.

[7] H. Schlichting and K. Gersten. *Boundary-Layer Theory*. Springer - Originally published by McGraw Hill - New York - 1979, 1979 8th ed. 2000.